REPORT DOCUMENTATION PAGE

Form Approved
OMB No. 0704-0188

PLEASE DO NOT RETURN YOUR FORM TO THE ABOVE ORGANIZATION.

1. REPORT DATE *(DD-MM-YYYY)*	2. REPORT TYPE	3. DATES COVERED *(From - To)*
08-10-2009	Journal Article	

4. TITLE AND SUBTITLE
Polarized Light in Coastal Waters: Hyperspectral and Multiangular Analysis

5a. CONTRACT NUMBER

5b. GRANT NUMBER

5c. PROGRAM ELEMENT NUMBER
0602782N

6. AUTHOR(S)
A. Tonizzo, J. Zhou, A. Gilerson, M.S. Twardowski, Derie Gray, Robert A Arnone, B. Gross, F. Moshary, S. Ahmed

5d. PROJECT NUMBER

5e. TASK NUMBER

5f. WORK UNIT NUMBER
73-9742-08-5

7. PERFORMING ORGANIZATION NAME(S) AND ADDRESS(ES)
Naval Research Laboratory
Oceanography Division
Stennis Space Center, MS 39529-5004

8. PERFORMING ORGANIZATION REPORT NUMBER
NRL/JA/7330-09-9176

9. SPONSORING/MONITORING AGENCY NAME(S) AND ADDRESS(ES)
Offiec of Naval Research
800 N. Quincy St.
Arlington, VA 22217-5660

10. SPONSOR/MONITOR'S ACRONYM(S)
ONR

11. SPONSOR/MONITOR'S REPORT NUMBER(S)

12. DISTRIBUTION/AVAILABILITY STATEMENT
Approved for public release, distribution is unlimited.

13. SUPPLEMENTARY NOTES

14. ABSTRACT
Measurements of the underwater polarized light field were performed at different stations, atmospheric conditions and water compositions using a newly developed hyperspectral and multiangular polarimeter during a recent cruise in the coastal areas of New York Harbor - Sandy Hook, NJ region (USA). Results are presented for waters with chlorophyll concentrations 1.3-4.8μg/l and minerals concentrations 2.0- 3.9mg/l. Angular and spectral variations of the degree of polarization are found to be consistent with theory. Maximum values of the degree of polarization do not exceed 0.4 and the position of the maximum is close to 100° scattering angle. Normalized radiances and degrees of polarization are compared with simulated ones obtained with a Monte Carlo radiative transfer code for the atmosphere-ocean system and show satisfactory agreement.

15. SUBJECT TERMS
inherent optical properties, polarization, hyperspectral

16. SECURITY CLASSIFICATION OF:			17. LIMITATION OF ABSTRACT	18. NUMBER OF PAGES	19a. NAME OF RESPONSIBLE PERSON
a. REPORT	b. ABSTRACT	c. THIS PAGE			Deric Gray
Unclassified	Unclassified	Unclassified	UL	18	19b. TELEPHONE NUMBER *(Include area code)* 228-688-7237

Polarized light in coastal waters: hyperspectral and multiangular analysis

Alberto Tonizzo[1], Jing Zhou[1], Alexander Gilerson[1,*], Michael S. Twardowski[2], Deric J. Gray[3], Robert A. Arnone[3], Barry M. Gross[1], Fred Moshary[1], Samir A. Ahmed[1]

[1]Optical Remote Sensing Laboratory, the City College and the Graduate Center of CUNY, New York, NY, 10031, United States
[2]Department of Research, WET Labs, Inc., 165 Dean Knauss Dr., Narragansett, Rhode Island, 02882, United States
[3]Naval Research Laboratory, Code 7333, Stennis Space Center, Mississippi, 39529, United States
**Corresponding author: gilerson@ee.ccny.cuny.edu*

Abstract: Measurements of the underwater polarized light field were performed at different stations, atmospheric conditions and water compositions using a newly developed hyperspectral and multiangular polarimeter during a recent cruise in the coastal areas of New York Harbor - Sandy Hook, NJ region (USA). Results are presented for waters with chlorophyll concentrations 1.3-4.8μg/l and minerals concentrations 2.0-3.9mg/l. Angular and spectral variations of the degree of polarization are found to be consistent with theory. Maximum values of the degree of polarization do not exceed 0.4 and the position of the maximum is close to 100° scattering angle. Normalized radiances and degrees of polarization are compared with simulated ones obtained with a Monte Carlo radiative transfer code for the atmosphere-ocean system and show satisfactory agreement.

OCIS codes: (120.0280) Remote sensing and sensors; (010.4450) Oceanic optics; (260.5430) Polarization; (010.5620) Radiative transfer.

References and links

1. M. Chami, R. Santer, and E. Dilligeard, "Radiative transfer model for the computation of radiance and polarization in an ocean-atmosphere system: polarization properties of suspended matter for remote sensing," Appl. Opt. **40**, 2938-2416 (2001).
2. J. Chowdhary, B. Cairns, and L. D. Travis, "Contribution of water-leaving radiances to multiangle, multispectral polarimetric observations over the open ocean: bio-optical model results for case 1 waters," Appl. Opt. **45**, 5542-5567 (2006).
3. S. Sabbah, A. Lerner, C. Erlick, and N. Shashar, "Under water polarization vision-A physical examination," Recent Res. Dev. in Exp. Theoretical Biol. **1**, 123-176 (2005).
4. A. Gilerson, J. Zhou, M. Oo, J. Chowdhary, B. Gross, F. Moshary, and S. Ahmed, "Retrieval of fluorescence from reflectance spectra of algae in sea water through polarization discrimination: modeling and experiments," Appl. Opt. **45**, 5568-5581 (2006).
5. S. Ahmed, A. Gilerson, A. Gill, B. Gross, F. Moshary, and J. Zhou, "Separation of fluorescence and elastic scattering from algae in seawater using polarization discrimination," Opt. Commun. **235**, 23-30 (2004).
6. R. J. Peralta, C. Nardell, B. Cairns, E. E. Russell, L. D. Travis, M. I. Mishchenko, Michael, B. A. Fafaul, R. J. Hooker, "Aerosol polarimetry sensor for the Glory Mission," Proc. SPIE **6786**, 67865L (2007).
7. T. H. Waterman, "Polarization Patterns in Submarine Illumination," Science **120**, 927-932, (1954)
8. A. Ivanoff, N. Jerlov, T. H. Waterman, "A comparative study of irradiance, beam transmittance and scattering in the sea near Bermuda," Limnol. Oceanogr. **6**, 129-148 (1961).
9. V.A. Timofeeva, "On the problem of polarization of light in turbid media," Izvestiya Geophysics **5**, 766-774 (1961).
10. G. W. Kattawar and C. N. Adams, "Stokes vector calculations of the submarine light field in an atmosphere-ocean with scattering according to a Rayleigh phase matrix: effect of interface refractive index on radiance and polarization," Limnol. Oceanogr. **34**, 1453-1472 (1989).
11. G. W. Kattawar, "Polarization of light in the ocean," in *Ocean Optics*, R.W. Spinrad, K. L. Carder and M. J. Perry eds. (Oxford University Press, New York, 1994).
12. K. J. Voss and E. S. Fry, "Measurement of the Mueller matrix for ocean water," Appl. Opt. **23**, 4427-4439 (1984).

#106439 - $15.00 USD Received 16 Jan 2009; revised 16 Mar 2009; accepted 24 Mar 2009; published 25 Mar 2009

13. T. W. Cronin and N. Shashar, "The linearly polarized light field in clear, tropical marine waters: spatial and temporal variation of light intensity, degree of polarization and e-vector angle," J. Exp. Biol. **204**, 2461-2467 (2001).
14. A. Lerner, E. H. Carynelisa, S. Nadav, S. Shai, "On the quest for the scattering mechanism that determines the polarization," presented at the Ocean Optics XVIII, Montreal, Canada, October 9-13, 2006.
15. M. Chami, "Importance of the polarization in the retrieval of oceanic constituents from the remote sensing reflectance," J. Geophys. Res. **112**, C05026 (2007).
16. M. Chami and D. McKee, "Determination of biogeochemical properties of marine particles using above water measurements of the degree of polarization at the Brewster angle," Opt. Express **15**, 9494-9509 (2007).
17. K. L. Coulson, *Polarization and intensity of light in the atmosphere* (Deepak Publishers, Hampton, VA, 1988).
18. G. Mie, "Beitrage zur optik truber medien, speziell kolloidalen metal-losungen," Ann. Phys. **25**, 377-442 (1908).
19. N. Shashar, S. Sabbah, T. W. Cronin, "Transmission of linearly polarized light in sea water implications for polarization signaling," J. Exp. Biol. **207**, 3619-3628 (2004).
20. A. Gilerson , A. Tonizzo, J. Zhou, R. Dyer, J. Chowdhary, B. Gross, F. Moshary, S. Ahmed, "Characterization of multi-angular hyperspectral polarized reflectance from coastal waters," Proc. SPIE **7105**, 710509 (2008).
21. R. W. Gould Jr., R. H. Stavn, M. S. Twardowski, and G. M. Lamela, "Partitioning optical properties into organic and inorganic components from ocean color imagery," in *Ocean Optics XVI*, S. Ackleson and C. Trees, eds. (Office of Naval Research CDROM, 2002).
22. J. M. Sullivan, M. S. Twardowski, P. L. Donaghay, S. A. Freeman, "Use of optical scattering to discriminate particle types in coastal waters," Appl. Opt. **44**, 1667-1680 (2005).
23. M. S. Twardowski, C. Moore, M. Slivkoff, J. Sullivan, S. Freeman, J.R.V. Zaneveld, "Volume Scattering Functions for Selected Ocean Waters: Revisited." Progress in Oceanography, in press.
24. T. J. Petzold, "Volume scattering functions for selected ocean waters," Tech. Rep. SIO 72-78 (Scripps Institution of Oceanography, San Diego, Calif., 1972).
25. C. D. Mobley, *Light and Water: Radiative Transfer in Natural Waters* (Academic, New York, 1994), Chap. 3.
26. E. Hecht, *Optics* (Addison-Wesley, Freeport, NY, 1998) Chap. 8.
27. J. Ramella-Roman, S. Prahl, and S. Jacques, "Three Monte Carlo programs of polarized light transport into scattering media: part I," Opt. Express **13**, 4420-4438 (2005).
28. A. Morel and B. Gentili, "Diffuse reflectance of oceanic waters: its dependence on Sun angle as influenced by the molecular scattering contribution," Appl. Opt. **30**, 4427-4438 (1991).
29. J. T. Adams and G. W. Kattawar, "Neutral points in an atmosphere-ocean system. 1: Upwelling light field," Appl. Opt. **36**, 1976-1986 (1997).
30. J. T. Adams, E. Aas, N. K. Hojerslev, B. Lundgren, "Comparison of radiance and polarization values observed in the Mediterranean Sea and simulated in a Monte Carlo model," Appl. Opt. **41**, 2724-2733 (2002).
31. World Climate Research Program (WCRP), "A Preliminary Cloudless Standard Atmosphere for Radiation Computation" (International Association for Meteorology and Atmospheric Physics, Boulder, CO, 1984).
32. C. Cox and W. Munk, "Statistics of the sea surface derived from sun glitter," J. Mar. Res. **13**, 198-227 (1954).

1. Introduction

Polarization characteristics of underwater light contain useful additional information on inherent optical properties (IOP), concentrations and size distributions of water constituents when compared with standard reflectance data [1-5]. In particular, information on the state of the water constituents can be obtained through analysis of the spectral and geometrical angular dependence of the polarized light components. In addition, this analysis can help assess visibility in underwater environments, provide interpretation of ocean lidar signals, etc. These properties should also be taken into account in the studies of atmospheric aerosols above ocean which employ polarization properties of atmospheric particulates [6].

Although many measurements of light scattering in the seawater have been made, the majority of them have not taken in consideration the changes that occur in the linear polarization of the light field. Despite the importance of polarization for marine applications, relatively few *in situ* observations of the oceanic polarization state of light have been carried out, owing to a lack of instrumentation and to the practical difficulties in achieving reliable measurements. Watermann [7] was the first to measure the polarized light field under water and showed its dependence on the solar zenith angle and the viewing azimuthal angle. Watermann's pioneering work was followed by Ivanoff *et al.* [8] and Timofeeva [9], whose

#106439 - $15.00 USD Received 16 Jan 2009; revised 16 Mar 2009; accepted 24 Mar 2009; published 25 Mar 2009

studies, combining both laboratory measurements and underwater measurements in natural environments, highlighted the effects of various particulate properties (both organic and inorganic) on the polarization of the underwater light field. In the 1980's and 90's, a large amount of theoretical modeling of the underwater polarization was carried out. Much interest was focused on the calculation of Stokes vectors and Mueller matrices to determine the scattering properties of suspended particles and the effects of the air-water interface on the underwater polarized light [10, 11]. Noteworthy exceptions to the theoretical work are the experimental measurements obtained by Voss and Fry [12], who developed their own electro-optic light scattering polarimeter to measure the Mueller matrices of water samples.

In the last decade, studies related to the underwater light field have been gradually emerging again. This definitely includes the work of Cronin and Shashar [13, 3] who were the first to provide hyperspectral polarization measurements at various zenith and azimuthal viewing angles. Their investigations described the mechanisms of polarization vision in underwater environments focusing on visually mediated tasks performed by polarization sensitive animals. However, due to the fact that measurements were mainly taken in clear waters, the effect of suspended particles was not taken in consideration. Lerner *et al.* [14], following the work of Cronin and Shashar, reported polarization measurements not only in clear waters but also in presence of a phytoplankton bloom (moderately turbid waters). Reported data showed high instability of the percent polarization in the presence of Mie scatterers (as was the case of the phytoplankton bloom). The calculated values, while nicely reproducing the shape of the degree of linear polarization (DOP) in clear water conditions, didn't show the same instabilities. This is probably due to the fact that the instrument had to be manually adjusted to the desired azimuth and elevation positions; therefore it wasn't suitable for the rapidly changing underwater environment.

Remote sensing of ocean water provides information on suspended particles. Among the different types of suspended matter in ocean water, phytoplankton plays the primary role in global biological production in the ocean and, therefore, in the carbon cycle. Remote sensing measurements of ocean color are directly related to the water leaving spectral radiance which depends on the absorption and scattering properties of the suspended particles. However, phytoplankton cells exhibit only weak polarization effects (because of the small index of refraction relative to water) while inorganic particles, which are strong backscatters, appreciably affect the polarization signal [1]. Having this in mind, Chami [15] investigated the influence of marine particles on the polarized radiation exiting the ocean. Using theoretical modeling he showed that an empirical-based inversion approach relying on the underwater polarized radiance could retrieve the concentration of inorganic particles regardless of the phytoplankton content in coastal waters. On this basis, Chami and McKee [16] also performed *in situ* measurements of the polarization state of underwater oceanic radiation with the purpose of having direct estimation of suspended inorganic matter concentration from remotely sensed data in coastal waters. REFPOL, the instrument used in these measurements, was a multispectral radiometer with only four channels centered at 450, 650, 850 and 1650nm together with polarizers which rotate in front of the detectors, allowing for successive (not simultaneous) measurements of radiance values.

In this paper we set out to fill the gaps in previous studies to obtain a comprehensive understanding of the changes that occur in the polarized light in coastal waters. Unlike previous multiband instruments, we will obtain underwater angularly resolved hyperspectral measurements of the DOP in coastal environments illustrating how the variability of the DOP is connected to water constituents. Measurements were also taken in different atmospheric conditions, to observe the effects of diffuse light, rather than direct sun light on the DOP and a comparison between above and underwater measurements is explored. Finally, we assess the consistency between our measurements and theoretical polarized radiative transfer models regarding the influence of marine particles on the polarized signal with particular emphasis on the corresponding wavelength and angular dependence.

In Section 2, the needed definitions and geometrical angles are given and the principles of the relevant scattering processes are discussed. In Section 3, the field experiments will be

#106439 - $15.00 USD Received 16 Jan 2009; revised 16 Mar 2009; accepted 24 Mar 2009; published 25 Mar 2009

described and the operating principles of the hyperspectral polarimeter introduced. In Section 4, measurements of the DOP will be presented and discussed together with corresponding *in situ* standard optical measurements, including total reflectance spectra (GER Spectroradiometer) and water absorption and attenuation spectra (WET Labs AC-9 instrument). In Section 5, field data are compared with simulations obtained using a Monte Carlo radiative transfer code of the atmosphere-ocean system. Both radiance and DOP in the principal plane obtained with the Monte Carlo simulations are presented. Because the solar angle, surface wind speed and detector depths were recorded along with the radiance and polarization value, to perform these simulations, only a few assumptions need to be made about the scattering characteristics of the water.

2. Theoretical background

The polarization state of the underwater light field is quantified using the Stokes vector $S = [I\ Q\ U\ V]$, where I represents the energy flux ($Wm^{-2}nm^{-1}$), Q and U describe the linearly polarized component of this flux, while its circular polarized component is described through the Stokes parameter V. Except for circular/elliptical polarization next to the borders of Snell's window (which is the circular region above an underwater observer with an aperture equal to twice the critical angle, $\theta_c = 48.6°$), the underwater light field is essentially linearly polarized [8]. The DOP is a measure of the percentage of linear polarization and can be expressed as:

$$DOP = \frac{\sqrt{Q^2 + U^2}}{I}. \tag{1}$$

Oceanic water, especially in the coastal areas, contains many suspended particles (inorganic and organic particles, which include living and nonliving varieties and even air bubbles). Scattering processes clearly modify the polarization state and the angular features of the polarized light (*i.e.* their dependence on the scattering angle, the angle between the incoming light and the direction of observation), are strongly related to the size, shape and composition (*i.e.* refractive index) of their scattering sources.

In the real atmosphere, Rayleigh scattering by molecules is the dominant process affecting the observed polarization and the contribution of the aerosols can be considered as a first-order correction to the pure Rayleigh atmosphere [17]. In the case of single Rayleigh scattering by spherical particles, the DOP of scattered light is minimal (actually zero if the incoming beam is 100% unpolarized) at scattering angles of 0° and 180°. In contrast, the scattering in the orthogonal plane (90° and 270°) eliminates the in-plane polarization component so that the DOP is maximized with a value of 1. Multiple scattering, however, depolarizes the signal, causes a decrease of the DOP and the appearance of neutral points in the DOP distribution.

However, in the ocean environment, scattering by water and suspended particles is the dominant process. Assuming the shape of each scattering sources in the ocean to be spherical, and the composition of each scattering source to be represented by a single value of the refractive index, the scattering properties of these particles can be computed relatively easily using Mie theory in assumption that the size distributions and the refractive indices are known [18]. In the case of Mie scattering, the DOP of scattered light is also minimal in the forward and backward directions; however, increasing concentrations of chlorophyll affect the spectral behavior of the DOP (for specific spectral intervals, hence the necessity of a hyperspectral analysis), and multiple scattering effects, due to increasing concentrations of minerals, can shift the maximum of the DOP toward 100° scattering angles [1]. Figure 1 shows the relevant scattering and geometric angles we use in describing our measurements.

#106439 - $15.00 USD Received 16 Jan 2009; revised 16 Mar 2009; accepted 24 Mar 2009; published 25 Mar 2009

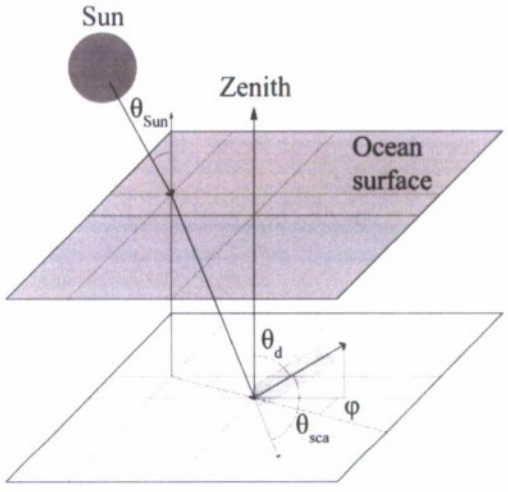

Fig. 1. Geometry of observation. θ_{Sun} is the solar zenith angle; θ_d is the detector, or viewing zenith angle; θ_{sca} is the scattering angle; φ is the detector azimuthal angle.

3. Instruments and methods

3.1 The polarimeter

Polarization measurements were taken using a hyperspectral and multiangular polarimeter developed by the Optical Remote Sensing Laboratory at the City College of New York, NY. The instrument consists of three Satlantic Hyperspectral radiance sensors (recording intensity at the wavelengths 350-800nm, 8.5° in-water field of view) mounted on a scanning system controlled by an underwater electric stepper motor as shown in Fig. 2. The heads of the sensors are positioned on the pivot point of the motor, in this way measurements are always taken at the same depth and the volume of water immediately nearby the heads of the sensor, which usually contributes the majority of the recorded signal, was the same for all angles. The motor rotates the sensors in a vertical plane in a specific angular range which was adjusted according to the solar zenith angle in order to cover the full 0-180° range of scattering angles. Measurements were taken every 5°. Linear polarizers are attached in front of the sensors with orientations at 0° (vertical), 90° (horizontal) and 45°.

From these measurements, the analysis of total radiance and DOP is obtained [19]. Briefly, if I_0, I_{90}, I_{45} are the intensity values recorded by the three Satlantic sensors, then the total intensity (which corresponds to the Stokes parameter I) is given by:

$$I = I_0 + I_{90}\,. \tag{2}$$

while the DOP is given by:

$$DOP = \frac{\sqrt{(I_0 - I_{90})^2 + (2I_{45} - I_{90} - I_0)^2}}{I}\,. \tag{3}$$

By rotating the sensors relative to the nadir direction, the instrument scanned the angular features of the underwater DOP in a vertical plane defined by its azimuth angle relative to the sun. The azimuth angular orientation of the instrument can be easily controlled by hand with an accuracy of 5°. The initial azimuth angular position usually corresponds to the principal plane, which is defined by the sun and the zenith. During this cruise all measurements were recorded only in the principal plane (*i.e.* φ = 0°). We exploited all the features of our instrumentation (*i.e.* the possibility of measuring at different azimuth angles and at different depths) during its initial testing in chlorophyll rich waters [20]. If measurements are taken in

#106439 - $15.00 USD Received 16 Jan 2009; revised 16 Mar 2009; accepted 24 Mar 2009; published 25 Mar 2009

the principal plane (in which the Stokes parameter $U = 2I_{45}-I_{90}-I_0 = 0$), only the outputs of the sensors with polarizers oriented at 0° and 90° are needed for the calculation of the DOP and a simplified version of equation (3) can be used:

$$DOP = \frac{I_0 - I_{90}}{I}. \quad (4)$$

Data are acquired through a customized Labview program which automatically controls the rotation of the electric stepper motor synchronized with the data acquisition of the hyperspectral sensors. The method of data collection allows us to measure simultaneously and in real-time the hyperspectral radiance values recorded by all the sensors as the stepper motor rotates. The total angular sampling time was approximately 10-15 minutes depending on the integration time required to obtain noise-free measurements. Even though the duration of the total acquisition time should be decreased to reduce the strong variability in the optical properties of particles that can be found in highly dynamic coastal ecosystems, the variability of the data points recorded with the WET Labs AC-9 package never exceeded 20%, therefore we assumed no major changes in the water conditions during the sampling time. Typical values of the integration time ranged between 0.2 and 2s per recording, depending on scattering angles and atmospheric conditions. Several recordings were taken for each angle to obtain the averaged value of the intensity.

3.2 Field measurements methodology

Data were collected during a recent cruise on the R/V "Connecticut" in the coastal areas of New York Harbor - Sandy Hook, NJ region (USA), on July 21-23 2008. The data reported in this paper were collected at eight stations. The coordinates of each station, the corresponding solar zenith angles (θ_{Sun}), the wind speeds and the times of the day are given in Table 1.

Table 1. Coordinates and solar zenith angles of the sampling stations.

Station	Longitude	Latitude	θ_{Sun}	Wind speed	Starting time
1	73°53'658"W	40°26'978"N	21±1°	2.5m/s	12^{30}
2	73°53'066"W	40°27'975"N	57±2°	3.8m/s	16^{15}
3	73°52'202"W	40°23'509"N	36±2°	5.5m/s	9^{40}
4	73°54'002"W	40°26'905"N	22±2°	3.2m/s	12^{45}
5	73°47'387"W	40°29'646"N	56±2°	4.8m/s	16^{10}
6	74°08'727"W	40°29'758"N	28±2°	6.4m/s	10^{30}
7	74°08'727"W	40°38'023"N	21±1°	8.1m/s	12^{30}
8	75°03'445"W	41°30'843"N	46±2°	8.0m/s	15^{15}

The instrument was lowered from a winch extending from the side of the ship (approximately 3-4m from the side of the ship) so that shadow effects were minimized. The principal plane was approximately normal to the ship axes and the sun was on the side of the instrument. The entire assembly was kept 1m below the water surface using four arms with buoys attached (Fig. 2(c)). This configuration also allowed the scanning system to always rotate in a plane perpendicular to the water surface. For normalization purposes, downwelling irradiance was also recorded with a Satlantic Hyperspectral irradiance sensor positioned on the front deck of the ship. The wind speed according to the ship instrument measurements, as shown in Table 1, was in the range 2.5 to 8.1m/s and the ocean surface wave amplitude did not exceed 1.2m. The sky was clear blue with no clouds during the data acquisition time for the first two days (Stations 1-5) and overcast during the last day (Stations 6-8). Water optical properties were measured at the same stations by an AC-9 instrument (WET Labs, Inc.). Attenuation and absorption data are available for Stations 1, 4, 5 and 7. Concentrations of mineral particles and chlorophyll were not measured directly in the field, but they can be estimated by analyzing absorption and attenuation spectra measured with our AC-9 instrument. Specifically, the total scattering coefficient at 555nm, which is defined as the difference between total attenuation

#106439 - $15.00 USD Received 16 Jan 2009; revised 16 Mar 2009; accepted 24 Mar 2009; published 25 Mar 2009

and absorption coefficients, is a good approximation for TSS (Total Suspended Solids) based on previous studies [21]. Minerals concentration then can be approximated as TSS concentration multiplied by 0.76 [21]. Chlorophyll concentration, on the other hand, can be estimated as the elevation from the baseline at 675 nm on the absorption spectrum divided by an *in vivo* specific absorption for chlorophyll of $0.0146 m^2 mg^{-1}$ [22]. Understanding that these assumptions can strongly differ for different regions and waters, we used them only as a rough approximation for chlorophyll and minerals concentrations.

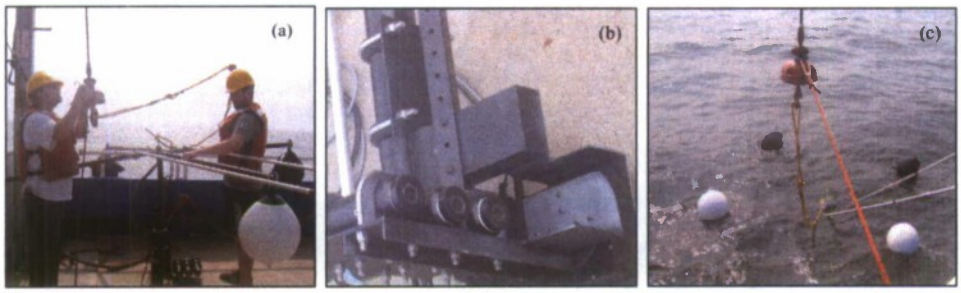

Fig. 2. The underwater instrument developed by the Optical Remote Sensing group at City College of New York. (a) The instrument on the deck of R/V "Connecticut", (b) a detail of the Satlantic Hyperspectral sensors, (c) the instrument under water.

4. Experimental results

4.1 Characterization of water compositions

Attenuation (c) and absorption (a) curves with and without water are shown in Fig. 3, minerals and chlorophyll concentrations estimated using the above approximations are summarized in Table 2. In Fig. 3(c) total absorption spectra (a_{tot}) are shown which include water absorption together with the spectra from Fig. 3(a). As will be shown below, *a priori* knowledge of the total absorption and attenuation spectra are important in the spectral analysis of the DOP.

We also recorded total reflectance spectra just below the water surface, using a fiber optic probe attached to a GER spectroradiometer (Fig. 4). As mentioned earlier, the sky was clear with no clouds at Stations 1-5 while at Stations 6-8, the sky was overcast resulting in mostly diffuse incident light. Station 7 was located at the entrance of the Hudson River and Station 8 was located further up the river which explains the strong increase of reflectance (especially for Station 8) due to an increase of mineral scattering.

Table 2. Minerals and chlorophyll concentrations estimations.

	St1	St4	St5	St7
Minerals (mg/l)	2.5	3.2	2.0	3.9
Chlorophyll (µg/l)	4.8	3.9	1.3	2.1

4.2 Measurements of particle phase functions

Along with the absorption and attenuation coefficients, the volume scattering function (VSF) is one of the fundamental IOPs which govern the propagation of polarized light in aquatic environments. VSF measurements were made with a custom device called the MASCOT [23]. It uses a 658 nm laser diode source and 17 independent detectors to measure volume scattering from 10 to 170° in 10° increments. Sampling rate for all detectors is 20Hz. A wedge depolarizer installed in front of the source provides unpolarized incident irradiance. Independent silicon diode detectors allow resolution of the VSF without any moving parts, with each detector gain optimized for its specific angular measurement. Based on curvature in

#106439 - $15.00 USD Received 16 Jan 2009; revised 16 Mar 2009; accepted 24 Mar 2009; published 25 Mar 2009

the VSF at specific angles, relative nominal scattering intensities, and the need to avoid stray light contamination, detector field-of-views (FOVs) are set at 0.8°, 2°, 3° and 4° for the 10°, 20°, 30° and 40° measurements, respectively. Detectors at other angles have a FOV of 5°. Calibration and validation of MASCOT VSF measurements were carried out with microspherical beads traceable to NIST standards. Angular weighting functions were computed numerically for each angle measurement. Beam attenuation was used to correct for light losses along the optical path of the MASCOT scattering measurements (all pathlengths nominally ~20cm). Normalized particle phase functions (PPFs) are calculated from the VSFs values divided by the scattering coefficient at 650nm (obtained from the difference between attenuation and absorption at 650nm measured with our AC-9 instrument). The PPF for Station 1 is compared with the standard Petzold's phase function [24]. Specifically, the three phase functions corresponding to each water type are averaged to produce a representative particulate phase function, as described by Mobley [25]. Figure 5 shows the comparison between MASCOT and Petzold's phase functions. Similar results are obtained for Stations 4, 5 and 7, due to similar water compositions. The agreement between MASCOT measurements and Petzold's functions, justifies the choice of the latter to represent the phase functions of particulate matter in the model described in Section 5.

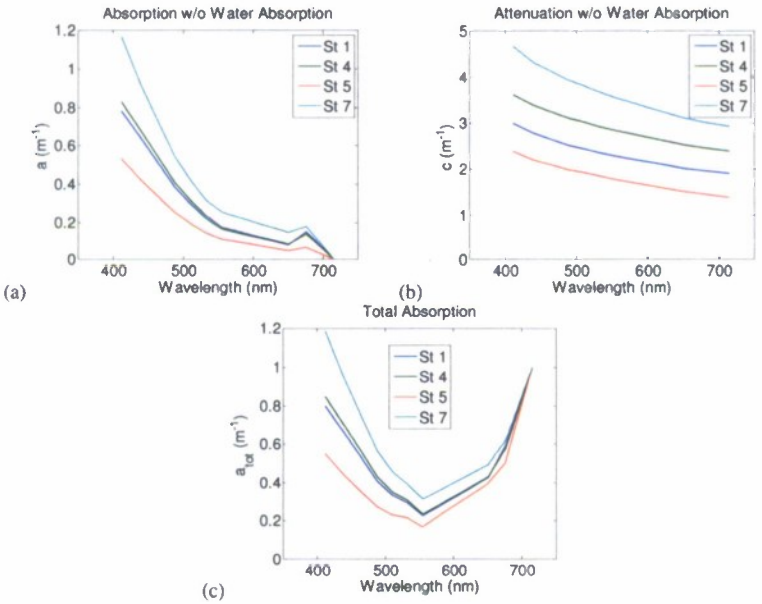

Fig. 3. Absorption and attenuation spectra recorded with the WetLabs package.

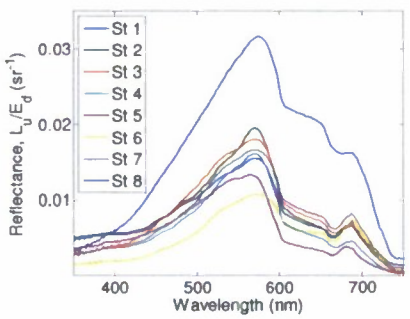

Fig. 4. GER total reflectance spectra.

#106439 - $15.00 USD Received 16 Jan 2009; revised 16 Mar 2009; accepted 24 Mar 2009; published 25 Mar 2009

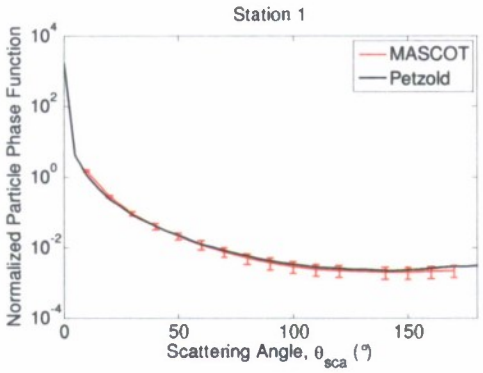

Fig. 5. Comparison of MASCOT measurements and standard Petzold functions.

4.3 Results of polarization measurements

To begin, we wish to verify the polarization state of the water under specialized illumination conditions. Figure 6(a) is an example (obtained when scattering angle is 0°, which corresponds to the sensors looking directly at the underwater sun light) where the DOP is effectively 0 since there's no difference in readings between the three polarization directions. In this case, the impact of atmospheric particles and air-water interface on underwater polarization was minimal, while for scattering angles away from 0 and 180° (90°, for example) the situation changes dramatically (Fig. 6(b)).

All recorded DOP values are based on measurements of radiances with different polarizers in front of the sensors. The dependence of these radiances (*i.e.* vertical, horizontal and 45°) as well as of the total radiance normalized to the downwelling irradiance as a function of the scattering angle is shown in Fig 7. The maximum differences are around 100° which corresponds to the maximum of the DOP. Relationships of these dependencies with the volume scattering functions should be further investigated.

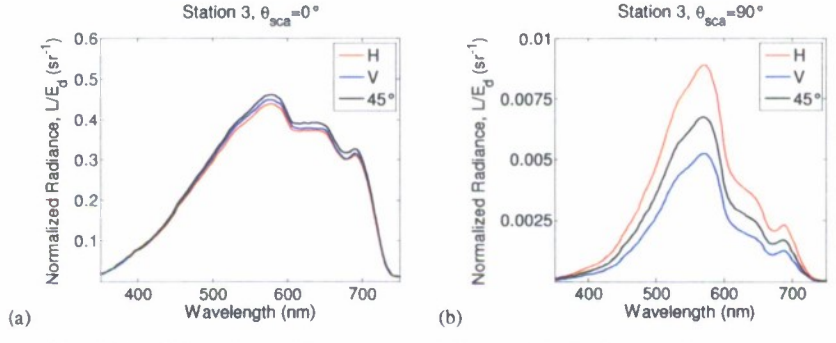

Fig. 6. Spectral dependence of the signal recorded by the Satlantic Hyperspectral sensors when the scattering angle is 0° (a) and when it's 90° (b). The instrument is positioned in the main scattering plane, 1m below water.

#106439 - $15.00 USD Received 16 Jan 2009; revised 16 Mar 2009; accepted 24 Mar 2009; published 25 Mar 2009

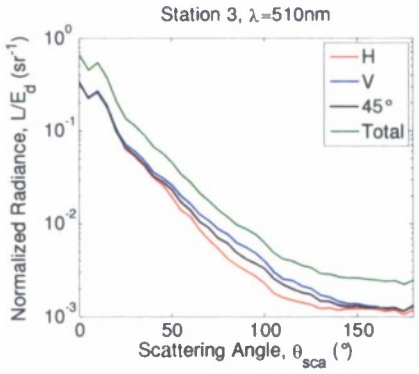

Fig. 7. Dependence of normalized radiance components on the scattering angle

In assessing our polarization measurements for stability, we took multiple measurements when possible. Clearly measurement errors can occur due to the changing ocean environment and can be amplified when DOP values are small. Figure 8 shows the DOP for all data points acquired for a set of representative measurements, corresponding to Station 1. Note the low variability of the experimental data points for most of angles underlining the high accuracy of the detection method. We attribute this to the positioning of the entire assembly on four buoys, which kept the sensors approximately at the same depth even in conditions of high waves. For scattering angles inside Snell's window (*i.e.* between 0 and 65° scattering angle, for Station 1), the largest fluctuations induced by surface waves were observed.

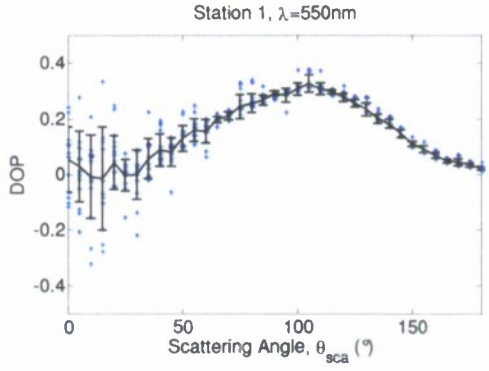

Fig. 8. Spread of the data points acquired during a set of measurements. Data are shown for Station 1, λ=550nm.

To assess our measurements, we first note that the DOP for ocean waters typically makes a bell-shaped distribution as function of the scattering angle with the maximum around 90° and going to zero in proximity of 0 and 180°. Typical plots of the DOP vs. scattering angle, recorded in the main scattering plane at 1m depth are presented in Fig. 9. The maximum of the DOP is lower than half the value predicted by Rayleigh theory (*i.e.* it reaches a maximum value of approximately 0.4 at 410nm). Results for Stations 1-5 are very similar due to similar water compositions and are represented by Station 1 and 2 in Fig. 9. However, we note a significant reduction of the DOP at Station 7 and 8 (Figs. 9(c) and 9(d)). These can be traced to the diffuse illumination from clouds as well as an increase in mineral concentrations (Station 8, see reflectance curve in Fig. 4). For reference, downwelling irradiance spectra for the same stations are shown in Fig. 9(e). An increased amount of suspended particles results

#106439 - $15.00 USD Received 16 Jan 2009; revised 16 Mar 2009; accepted 24 Mar 2009; published 25 Mar 2009

in increased number of multiscattering events, further depolarization and in turn lower DOP. We also note the shift of the maximum of the DOP towards 100° scattering angle. Chami *et al.* [1] predicted this effect and suggested its use to allow discrimination between biological and non-biological constituents which should be further verified. In fact, according to [3] as the real part of the refractive index increases (mineral particles) the absolute maximum of the DOP decreases in value and shifts towards higher scattering angles.

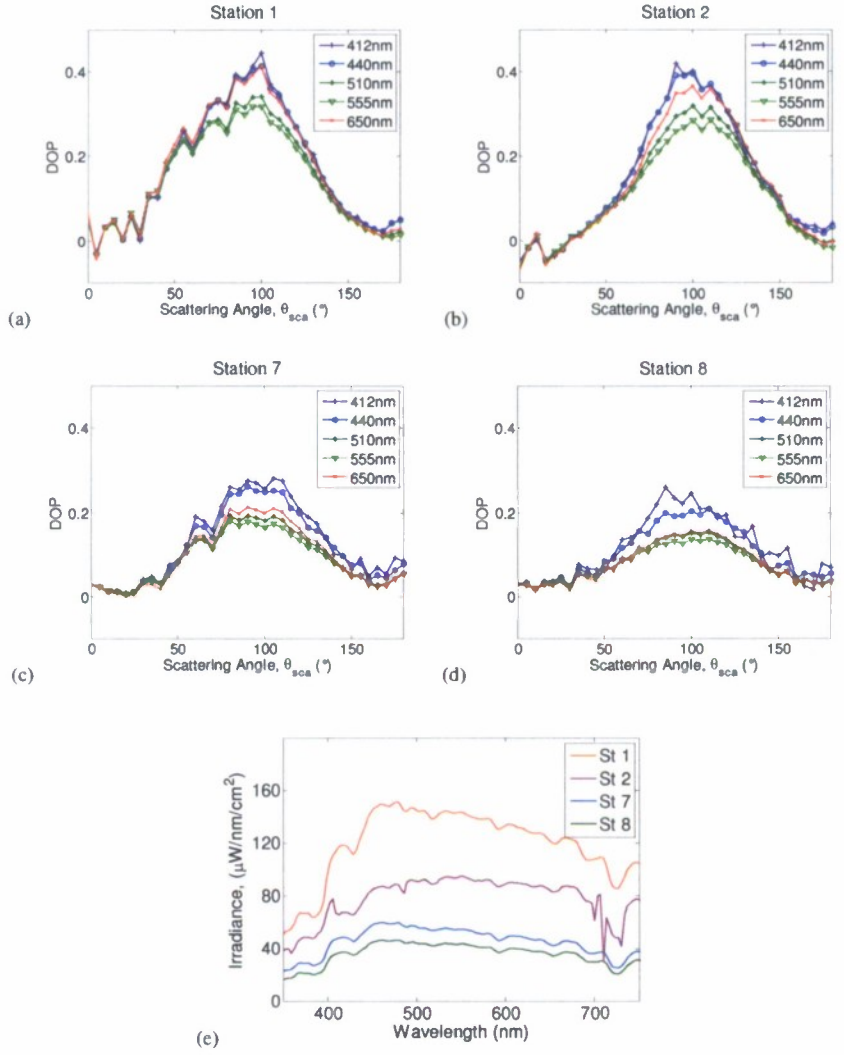

Fig. 9. (a)-(d) Plots of the DOP vs. scattering angle. The instrument is located in the principal plane 1m below water. (e) Downwelling spectral irradiance recorded at the same stations.

It's worth noting that for remote sensing purposes only scattering angles in the range 140-160° should be realistically considered. We recorded above water measurements for Station 4 and the data are presented in Fig. 10 in comparison with underwater measurements. For angles corresponding to in-water scattering angle less than 145° (since specular reflection of sun light occurs at ~147° in-water scattering angle, for Station 4) abnormally high values of DOP were observed, due to the contribution of the polarized reflected light. These values are not related to the characteristics of the water components; hence they are not shown in Fig.

#106439 - $15.00 USD Received 16 Jan 2009; revised 16 Mar 2009; accepted 24 Mar 2009; published 25 Mar 2009

10(a). On the other hand, for in-water scattering angle more than 145°, the reflection coefficients for the in-plane and out-of-plane polarizations are similar [26]; therefore the observed DOP is not due to reflection effects but to the polarization properties of the water-leaving radiance. From this it is clear that the DOP corresponding to the range 140-160° will not exceed 0.2. Taking into account the fact that Station 4 presented a relatively low concentration of minerals and the DOP decreases for higher concentration of minerals, we can assume this value of the DOP to be close to the upper limit which can be expected for remote sensing measurements in coastal waters. Values of DOP measured above and below water surface (Figs. 10(a) and 10(b)) for this range of angle well correspond to each other. The effect of absorption is not noticed here since the optical thickness of the water medium wasn't high enough to decrease the magnitude of the DOP measured above water (see Fig. 3(b)) [27], when compared with the underwater DOP. Swell and wind ruffling of the water surface affect much more the above water signal than the underwater measurements, as shown by the comparison of Figs. 10(a) and 10(b) curves. The former contain random sun glint reflections not present underwater. Above water recordings were performed while the instrument was held by the winch cable approximately 2-3m outboard from the ship, and 1m above water.

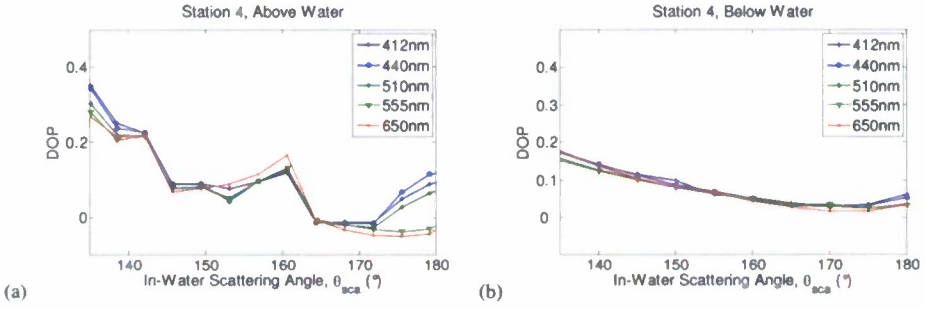

Fig. 10. Plots of the DOP vs. scattering angle for Station 4: (a) 1m above water, (b) 1m below water. The instrument is located in the principal plane.

The DOP was also found to vary with wavelength. Comparisons between spectral dependences for measurements of the DOP taken at different stations are presented in Fig. 11. In Fig. 11(a) (which corresponds to Station 1), we observe a maximum in the DOP at lower wavelengths. This region is dominated by chlorophyll and CDOM absorptions, as can be seen in Fig. 3(c) and in the normalized absorption spectrum, a_{norm}, (which is the total absorption normalized to the maximum total absorption) reported in the top part of Fig. 11(a). In the top part of Fig. 11(a) the total absorption spectrum (a_{tot}) divided by the total attenuation spectrum (c_{tot}) is also shown. Of course $a_{tot}/c_{tot}=1-\omega$, where ω, the single scattering albedo, is a good measure of the amount of multiple scattering. If ω decreases, multiple scattering events are reduced and the DOP increases. Figure 11(a) also shows that the DOP reaches maximum values in the range 0.4-0.5 at 410 and 440nm. On the other side of the spectrum (*i.e.* 700-750nm), another maximum appears. This behavior is consistent with the absorption spectrum. After 700nm, water absorption starts increasing, minimizing again elastic scattering. The relative maximum between 600-650nm is also consistent with the absorption curve. On both sides of this relative maximum, two minima occur and the DOP reaches minimum values around 0.3. The first minimum is consistent with the minimum in the absorption; absorption decreases and multiple scattering events increase, depolarizing the underwater light field. The second minimum, however, cannot be directly related to the absorption curve. This dip in the DOP is due to the chlorophyll fluorescence in this spectral interval, which occurs in addition to elastic scattering and which is unpolarized [4, 5]. This hypothesis is confirmed by the data recorded at Station 7 (Fig. 11(b)). In particular, within the Hudson River, the concentration of chlorophyll is very low, and the dip in the DOP is barely noticeable. In addition, the effect of chlorophyll fluorescence on the DOP is further confirmed by the comparison of experimental

#106439 - $15.00 USD Received 16 Jan 2009; revised 16 Mar 2009; accepted 24 Mar 2009; published 25 Mar 2009

data with Monte Carlo simulations, which will be shown in the next section. It's worth noticing that the spectral variations of the DOP and the effects of chlorophyll fluorescence are more pronounced at scattering angles where the DOP is close to maximum and weaker at other angles. In addition, below 400nm and above 700nm, because of the increasing water absorption, the absolute values of radiance become very small, leading to big uncertainties in the calculation of the DOP.

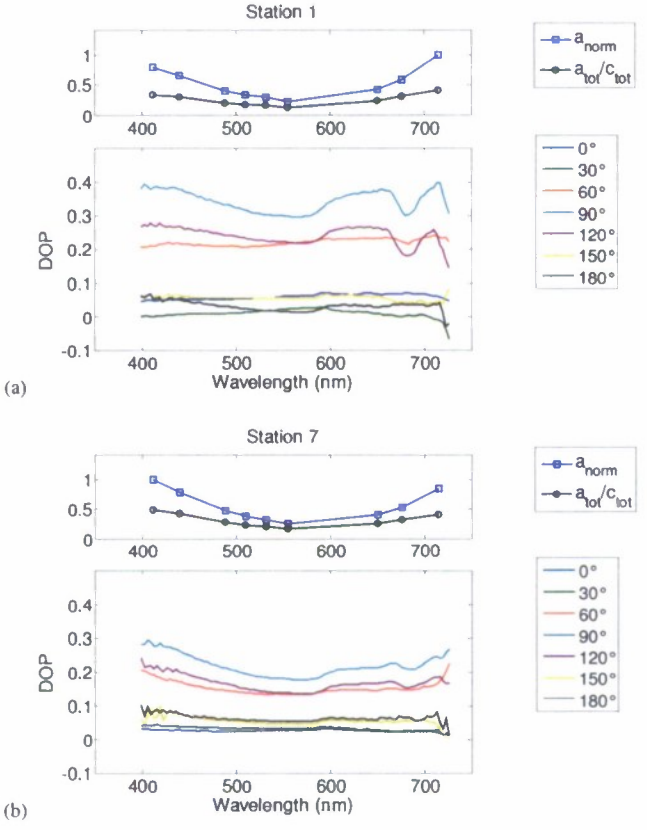

Fig. 11. Spectral dependence of the DOP: (a) Station 1 and (b) Station 7. The normalized total absorption spectrum (a_{norm}) and the total absorption spectrum divided by the total attenuation spectrum (a_{tot}/c_{tot}) are also shown.

5. Comparison of modeled and measured data

5.1 Description of the radiative transfer model

To assess the results beyond simple qualitative experiments, the polarimeter measurements were compared to the results of a Monte Carlo vector radiative transfer model. This is an updated version of the code used in Adams and Kattawar [28] and Adams *et al.* [29]. It is a plane-parallel model of the coupled atmosphere-ocean system and allows computation for a number of different layers in both the atmosphere and ocean. The specific details can be found in the above references, and we will only give a brief summary here. The atmosphere is modeled as a two-layer system. The top layer is assumed to be Rayleigh scattering only, while the bottom layer is a marine haze model comprised of Rayleigh plus aerosol scattering. The aerosol layer above the ocean surface is modeled using the MAR-I model published by the International Association for Meteorology and Atmospheric Physics [31]. The sea surface is

#106439 - $15.00 USD Received 16 Jan 2009; revised 16 Mar 2009; accepted 24 Mar 2009; published 25 Mar 2009

modeled using the sea-slope statistics of Cox and Munk [32]. In the water column, we use the dissolved and particulate absorption coefficients, the particulate scattering coefficient, and the absorption and scattering coefficients of pure ocean water. Light scattering in both the atmosphere and ocean is described by the elastic scattering Mueller matrix for each constituent. Atmospheric Rayleigh scattering is described using the Rayleigh matrix including depolarization factors. The aerosol matrix is found using the aerosol constituent parameters in a Mie code to produce the Mueller matrix. In the water, molecular scattering is again described using the Rayleigh matrix and the depolarization ratio for water. For particulate scattering, we use the averaged Petzold's particulate volume scattering phase function reported by Mobley [25]. To find a Mueller matrix for particulate scattering, we first define a reduced Muller matrix by dividing each element by the (1,1) element, the phase function. The particulate Mueller matrix is then obtained by assuming a hyperbolic particle size distribution with a slope of -4 and a constant relative index of refraction of $n=1.07+0.002i$, and calculating the reduced matrix using a Mie code. The result is that the reduced matrix is not much different than a reduced Rayleigh matrix, similar to that reported in Voss and Fry [12]. In all cases, atmosphere and ocean, the phase function and Mueller matrices are assumed to be independent of wavelength. Again, see reference [29] for the specific details and forms of the Mueller matrices.

The model was run for each wavelength of the AC-9 in-water measurements. The measured values of the dissolved and particulate values of the absorption and attenuation coefficients were used for the water column. The measured wind speed was used for the waveslope statistics (Station 1: 2.5m/s; Station 7: 8.1m/s). The largest unknown is the atmosphere. To determine the level of aerosols, we turned to the surface irradiance measurements shown in Fig. 9(e). The ratio of the measured surface irradiance to the extraterrestrial irradiance was found for each wavelength. In the model, the optical depth of the aerosol haze layer was varied until the modeled surface to top of the atmosphere ratio matched the measured one. Once this aerosol optical depth was found, the code was run for each wavelength and the Stokes vector parameters were found for a depth of 1m below the surface. These values were then divided by the calculated surface irradiance values to produce the normalized radiance reflectance.

5.2 Comparison between modeling and measurements.

Figure 12 shows a comparison between the measured and modeled values at Station 1 and 7, at a wavelength of 510nm for the DOP and the normalized radiance. Figures 12(a) and 12(b) compare the DOP and radiance at Station 1. The atmospheric optical depth at this wavelength was calculated to be 1.34, and values for the other wavelengths ranged from 1.0 to 2.0. The radiance values agree well, but there are differences, especially in the direction of the sun. The model tends to over predict the radiance in this direction, and then under predict it at larger angles. The most probable cause of this discrepancy is the generally unknown state of the atmosphere. By looking at the shape of the modeled radiance curve we guess that the incident skylight was more diffuse then the model predicts. The agreement between the magnitudes of the measured and modeled DOP is very good. At this shallow depth, one of the largest sources of uncertainty is the effect of the wind-blown surface. Though generally small in other azimuthal planes, in the principal plane, on the side containing the direct beam of the sun, increased wind speed will cause the direct solar beam to spread into more angles and in general reduce the maximum DOP. Modeled results for the same optical properties show that a smooth sea surface results in a maximum DOP approximately 5-10% higher than the wind-blown surface at Station 1.

Figures 12(c) and 12(d) show the comparisons at Station 7, also at a wavelength of 510nm. This day was overcast, and the atmospheric optical depth was calculated to be 8.98, with similar values for other wavelengths. Now it is unlikely that the atmospheric haze model correctly predicts the true nature of the atmosphere under these conditions, but we hypothesize that the light field incident on the ocean will be sufficiently diffuse that it doesn't make a great difference. The radiance values again show good agreement, though this time

#106439 - $15.00 USD Received 16 Jan 2009; revised 16 Mar 2009; accepted 24 Mar 2009; published 25 Mar 2009

the model tends to under predict the radiance at angles toward the sun. The DOP again agrees very well, though there is quite a bit of statistical noise in the Monte Carlo simulations due to the large atmospheric depth and very windy conditions.

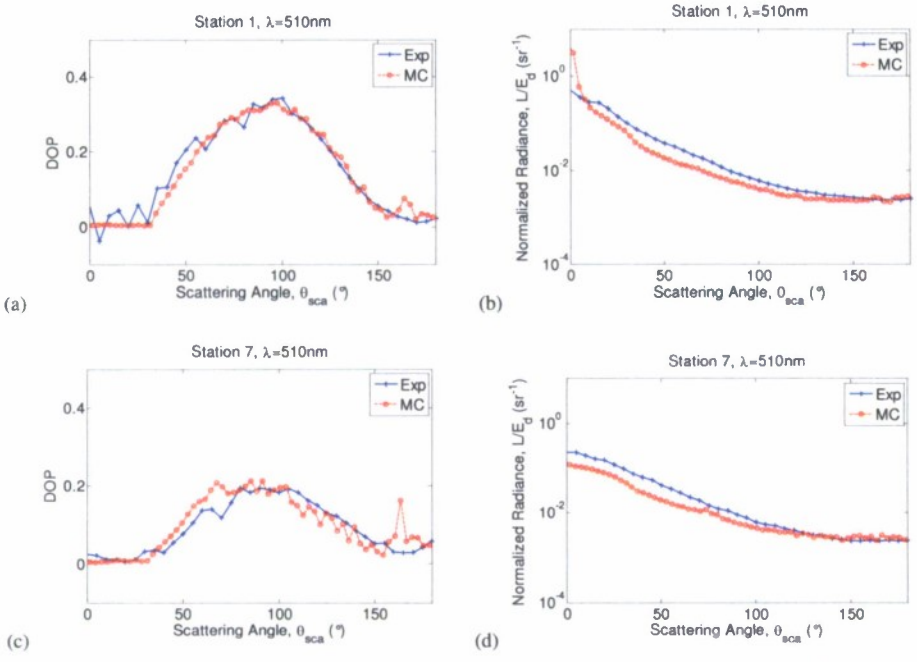

Fig. 12. Comparison of modeled and measured data for 510 nm, Station 1, (a) DOP, (b) normalized radiance. Station 7, (c) DOP, (d) normalized radiance.

The peak in the DOP curves near 180° is artifacts of the statistical nature of the Monte Carlo method. This is a well known issue when the solid angles become very small near the zenith direction, and there are insufficient upwelling photons traveling into these solid angles to resolve the DOP sufficiently. The peak observed in the Station 7 data is particularly noticeable.

Similar comparisons for a wavelength of 676nm are also presented in Fig. 13. The radiance curves match well, similar to the 510nm wavelength with similar discrepancies. But now the DOP match is poor. The Monte Carlo radiative transfer code didn't include chlorophyll fluorescence which, as hypothesized above, would decrease the value of the DOP.

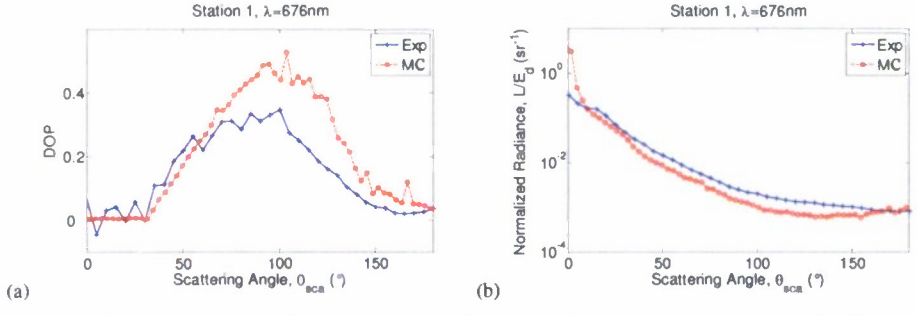

Fig. 13. Comparison of modeled and measured data for 676nm, Station 1, (a) DOP, (b) normalized radiance.

#106439 - $15.00 USD Received 16 Jan 2009; revised 16 Mar 2009; accepted 24 Mar 2009; published 25 Mar 2009

This probably explains the significant difference in the measured and simulated values. Figure 14 summarizes the spectral comparisons of modeled and measured DOP for four relevant scattering angles for Station 1. Again, the match is quite good except in the region of chlorophyll fluorescence as discussed before.

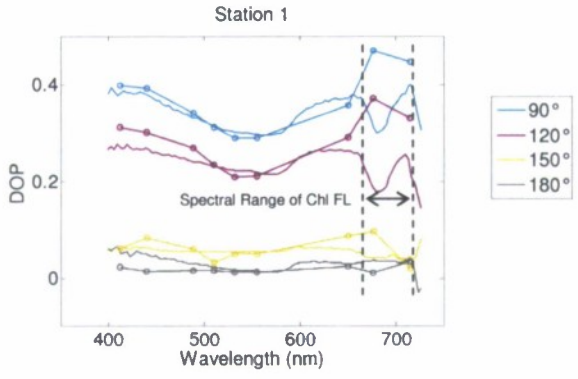

Fig. 14. Spectral comparison of modeled (circles) and measured (solid lines) DOP for four relevant scattering angles, Station 1.

6. Conclusions

Measurements of the polarization characteristics of coastal waters were acquired during a field experiment in the coastal areas of New York Harbor - Sandy Hook, NJ region (USA), using a newly developed hyperspectral and multiangular polarimeter. An analysis of the angular (0-180°) and spectral (400-750nm) variations of the degree of polarization was performed. It was observed that maximum values of the DOP, which occurred approximately at scattering angle of 100°, did not exceed 0.4 for all stations. In overcast conditions however, the light was still partially polarized but with the maximum DOP reduced to approximately 0.2.

Spectral dependence of DOP very well correlates with the measured water absorption and single scattering albedo (ω) spectra: increase of absorption (decrease of ω) corresponds to the decrease of the number of the scattering events which means less depolarization. These effects are more pronounced at scattering angles close to 90° where the DOP has its maximal values and almost unnoticeable at angles closer to 0 and 180°. In the spectral area of chlorophyll fluorescence we observed significant decrease of DOP which is explained by the depolarizing effect of fluorescence. Despite windy conditions at some stations where waves were up to 1.2m high, the angular profiles of the DOP and its maximal values remained similar to the values at the stations with the same water composition but lower wind speeds.

For remote sensing applications, when in-water scattering angles are in the range of 140-160°, the DOP does not exceed 0.2. In addition, we note that the measured values above water correctly correspond to the results of underwater measurements. This result suggests that, despite the effect of the water surface on the polarization of light, the contribution of the underwater polarized light field is sufficiently significant to affect the above water signal. This makes the study of polarization in the ocean promising for future improvement of retrieval algorithms in complex waters, such as those founded in the coastal areas. In addition, by performing these measurements underwater, further noise sources due to the wind-roughened state can be eliminated.

The agreement between the Monte Carlo results and the experimental data are also shown and clearly demonstrates the success of radiative transfer simulations applied to the transmission and scattering of light in an atmosphere-ocean system. The shape of both the radiance distribution and the DOP has been correctly reproduced for different atmospheric and water conditions.

#106439 - $15.00 USD Received 16 Jan 2009; revised 16 Mar 2009; accepted 24 Mar 2009; published 25 Mar 2009

It is expected that the ability of our polarimeter to provide information about the characteristics of the underwater polarized light field has great potential for application in radiative transfer problems in the earth-ocean system, especially if used in combination with other polarization-sensitive instruments recently developed; hyperspectral and multiangular data can be collected very accurately and in a relatively short time, thus changes both in the water and in the atmosphere can be avoided.

Acknowledgments

This research has been supported by grants from the Office of Naval Research, NASA and NOAA. Tom Legbandt of CCNY is warmly thanked for his time and patience, and for providing excellent technical assistance during the development of the polarization spectroradiometer, while benefiting from his full support, valuable guidance and positive creative ideas. We thank Scott Freeman for his precious help in the field and for his efficient assistance in the MASCOT supervision and data processing. We are especially grateful to James Adams for sharing his knowledge and code which proved to be indispensable in producing the modeled results. We are also very grateful to our reviewers, who took the time to carefully read our manuscript and make valuable corrections, additions, suggestions, and improvements.

#106439 - $15.00 USD Received 16 Jan 2009; revised 16 Mar 2009; accepted 24 Mar 2009; published 25 Mar 2009

#106439 - $15.00 USD Received 16 Jan 2009; revised 16 Mar 2009; accepted 24 Mar 2009; published 25 Mar 2009